12. The dissipation of $[Ca^{2+}]_i$ gradients will also contribute to the time of rise of fluorescence. An artifactual increase in fura 2 (fluo 3 was used in the present study) fluorescence that lasted 10 to 20 ms has been observed during the dissipation of gradients from the surface membrane to the center of chromaffin cells 20 μm in diameter [E. Neher and G. J. Augustine, *ibid.* **450**, 273 (1992)]. We have therefore calculated whether such an effect can explain the fluorescence changes reported here. A model for Ca^{2+} binding and buffering reactions that fits the time course of the evoked $[Ca^{2+}]_i$ transient has been presented elsewhere [C. W. Balke, T. M. Egan, W. G. Wier, *ibid.* **474**, 447 (1994)], and the appropriate equations describing diffusion from a point source were added. The changes in fluo 3 fluorescence associated with a Ca^{2+} spark for Ca^{2+} release fluxes of 4 pA (for 10 ms), 40 pA (for 1 ms), and 400 pA (for 0.1 ms) were then calculated. These fluxes resulted in similar peak normalized fluorescence (1.82, 1.93, and 1.91, respectively, averaged over a 2-μm region), but the rise times were quite different, peaking in 10.0, 1.6, and 1.1 ms, respectively. We conclude that the observed rise time of the fluorescence record cannot be explained by the dissipation of $[Ca^{2+}]_i$ gradients and therefore reflects the duration of SR Ca^{2+} release.
13. M. B. Cannell, H. Cheng, W. J. Lederer, *Biophys. J.* **67**, 1942 (1994).
14. Pharmacologically reducing the probability of SL Ca^{2+} channel opening also reduces the uniformity of the $[Ca^{2+}]_i$ transient in a way that is consistent with the idea that EC coupling is locally regulated by Ca^{2+} influx through Ca^{2+} channels (*13*) [M. B. Cannell, H. Cheng, W. J. Lederer, *J. Physiol.* **477**, 25P (1994); H. Cheng, M. B. Cannell, W. J. Lederer, *Circ. Res.* **76**, 236 (1995)]. Recently, it has been shown that alterations in I_{Ca} amplitude (by depolarization to different potentials) can also lead to spatial nonuniformity in $[Ca^{2+}]_i$(*23*), which further supports the idea that it is the local Ca^{2+} influx that determines the probability of activation of SR Ca^{2+} release.
15. H. Cheng, W. J. Lederer, M. B. Cannell, *Science* **262**, 740 (1993).
16. G. Meissner, *J. .Biol. Chem.* **261**, 6300 (1986); E. Rousseau, J. S. Smith, G. Meissner, *Am. J. Physiol.* **253**, C364 (1987).
17. The amplitude of the spontaneous Ca^{2+} spark could be explained by a number of SR release channels acting in concert as the conductance of a single RyR is barely sufficient to supply the calculated SR release flux (*15*). Several other lines of evidence suggest that SR release channels may be grouped together (*13*, *25*) in a functional unit. In skeletal muscle, anatomical evidence suggests that the RyRs may be clustered in the terminal cisterns of the SR [D. G. Ferguson, H. W. Schwartz, C. Franzini-Armstrong, *J. Cell Biol.* **99**, 1735 (1984)], whereas biochemical measurements indicate that the numbers of SL Ca^{2+} channels are insufficient to individually control RyRs (in cardiac myocytes) [D. M. Bers and V. M. Stiffel, *Am. J. Physiol.* **264**, C1587 (1993)]. If this is the case, the release of Ca^{2+} during a Ca^{2+} spark could be the result of the activation of a number of SR release channels acting in concert (*15*), which would then make up the release unit (*13*).
18. S. C. O'Neill, J. G. Mill, D. A. Eisner, *ibid.* **258**, C1165 (1990); A. W. Trafford, S. C. O'Neill, D. A. Eisner, *Pflueg. Arch.* **425**, 181 (1993).
19. T. F. McDonald, S. Pelzer, W. Trautwein, D. J. Pelzer, *Physiol. Rev.* **74**, 365 (1994).
20. The Na-Ca exchanger may stimulate SR Ca^{2+} release [N. Leblanc and J. R. Hume, *Science* **248**, 372 (1990); P. Lipp and E. Niggli, *J. Physiol.* **474**, 439 (1994)]. However, the voltage dependence of Na-Ca exchange {70 mV per e-fold change [E. Niggli and W. J. Lederer, *Nature* **349**, 621 (1991)]} does not match the observed voltage dependence of the spark rate. In addition, application of 100 μM Cd^{2+} (which blocks the I_{Ca}) prevents evoked Ca^{2+} sparks during the ramp depolarization.
21. At rest, the rate of spark production is about 1 s^{-1} in a line-scan image (*15*). Because a Ca^{2+} spark rate of 2.0 per 20 ms (Fig. 4) gives a spatial average increase in $[Ca^{2+}]_i$ of 17 nM at the end of the voltage ramp, we estimate that a Ca^{2+} transient of 1 μM would require an increase in Ca^{2+} spark rate of ~ 6 × 10^3 s^{-1}. If the probability of SR release channel opening is proportional to the square of the local $[Ca^{2+}]_i$ [S. Györke and M. Fill, *Science* **260**, 807 (1993)], then this increase in rate suggests that the local trigger $[Ca^{2+}]_i$ would be ~77 times the resting $[Ca^{2+}]_i$ or about 8 μM. Such high $[Ca^{2+}]_i$ will only occur close to open channels (*27*), so that all the channels within a release unit may be activated whereas those further away are not. Given this insensitivity of the RyR for $[Ca^{2+}]_i$ this calculation can also explain why a Ca^{2+} spark does not normally propagate (*15*) and suggests that the release unit is only effectively triggered by the local Ca^{2+} influx through a nearby SL Ca^{2+} channel.
22. Even at high local $[Ca^{2+}]_i$, SR release channels eventually close. This results from their intrinsic gating (note that their open probability must be <1). The mean open time of a release unit will depend on the physical organization of the channels in the unit (*25*) and on other factors that may influence the channel gating, such as phosphorylation state [H. H. Valdivia, G. Ellis-Davies, J. Kaplan, W. J. Lederer, *ibid.* **267**, 1997 (1995).
23. J. R. López-López, P. S. Shacklock, C. W. Balke, W. G. Wier, *J. Physiol.* **480**, 21 (1994)
24. Under near-physiological ionic conditions, the SR release channel current is about 2.2 pA [E. Rousseau and G. Meissner, *Am. J. Physiol.* **256**, H328 (1989)], whereas the SL Ca^{2+} channel's current is about 0.3 pA (*11*, *19*).
25. M. D. Stern, *Biophys. J.* **63**, 497 (1992).
26. The total flux associated with a channel opening is the single channel current multiplied by its open time. Our modeling and data suggest that the duration of Ca^{2+} release from a release unit is longer than the mean open time of a SL Ca^{2+} channel [<1 ms (*11*)]. Although Ca^{2+} release from an SR release unit is triggered by the opening of a SL Ca^{2+} channel, the release unit does not require the maintained presence of the SL Ca^{2+} influx because while it is open, the release within the unit is self sustaining (or regenerative). This regenerative behavior contributes to the release unit being open for a longer period of time than the SL Ca^{2+} channel (Fig. 5). We call this effect digital pulse stretching, by analogy with the use of monostables in digital electronics to produce longer pulses than their triggers. However, although regenerative, the release is not uncontrolled because the finite open time of the release unit effectively breaks the regenerative feedback loop.
27. We calculate that the local $[Ca^{2+}]_i$ 20, 80, and 180 nm from an open SR release channel (4 pA of Ca^{2+} flux) would be about 56, 18, and 7.7 μM, respectively. This local $[Ca^{2+}]_i$ would decay by half in 4.8, 211, and 765 μs, respectively, after channel closure. Thus the probability of a second channel in the release unit opening will depend on its distance from the first channel and will rapidly decline after closure of the first channel (*25*). The high local $[Ca^{2+}]_i$ needed to trigger the release unit comes from a nearby SL Ca^{2+} channel. However, because of the low conductance of SL Ca^{2+} channels (*24*), the Ca^{2+} channel that triggers a release unit must be even closer (within ~20 nm) to a RyR in the unit.
28. Supported by grants from NIH (HL36974 and HL25675), by Directed Research Initiative Funds awards from the Medical Biotechnology Center of the University of Maryland at Baltimore, and by the British Heart Foundation, London, UK.

31 October 1994; accepted 6 March 1995

Identification of hSRP1α as a Functional Receptor for Nuclear Localization Sequences

Karsten Weis, Iain W. Mattaj, Angus I. Lamond*

Import of proteins into the nucleus is a two-step process, involving nuclear localization sequence (NLS)–dependent docking of the substrate at the nuclear envelope followed by translocation through the nuclear pore. A recombinant human protein, hSRP1α, bound in vitro specifically and directly to substrates containing either a simple or bipartite NLS motif. hSRP1α promoted docking of import substrates to the nuclear envelope and together with recombinant human Ran reconstituted complete nuclear protein import. Thus, hSRP1α has the properties of a cytosolic receptor for both simple and bipartite NLS motifs.

Import of proteins into the nucleus is an active process consisting of at least two steps: first, the energy-independent docking of the substrate to the nuclear envelope, and second, translocation through the nuclear pore complex, which requires energy (*1*). The presence of a specific NLS in the imported protein is a prerequisite for both steps. In most cases the NLS consists either of a short domain of basic amino acids—for example, the simple NLS of SV40 T antigen (PKKKRKV)—or of two stretches of basic residues separated by a spacer of about 10 amino acids, the bipartite NLS motif (*2*).

A variety of biochemical and genetic approaches have been used to search for factors involved in nuclear protein import (*3*). Biochemical fractionation of import activities, by means of an in vitro transport assay (*4*), has shown that the two steps of nuclear protein import can be mimicked by two cytosolic fractions, A and B (*5*). Fraction B mediates the translocation step and consists of two protein components, Ran/TC4 and pp15 (*6*–*8*). Recently, importin has been identified as a *Xenopus* factor required for the first step of nuclear import (*9*). Importin is homologous to the yeast protein SRP1 (suppressor of RNA polymerase 1) (*10*). Factors that bind to the NLS motif in vitro are likely to play an important role in the import reaction. Such NLS-binding factors could either be free cytosolic proteins or could be associated with the nuclear envelope. Sever-

European Molecular Biology Laboratory, Meyerhofstrasse 1, Postfach 102209, D-69012 Heidelberg, Germany.

*To whom correspondence should be addressed.

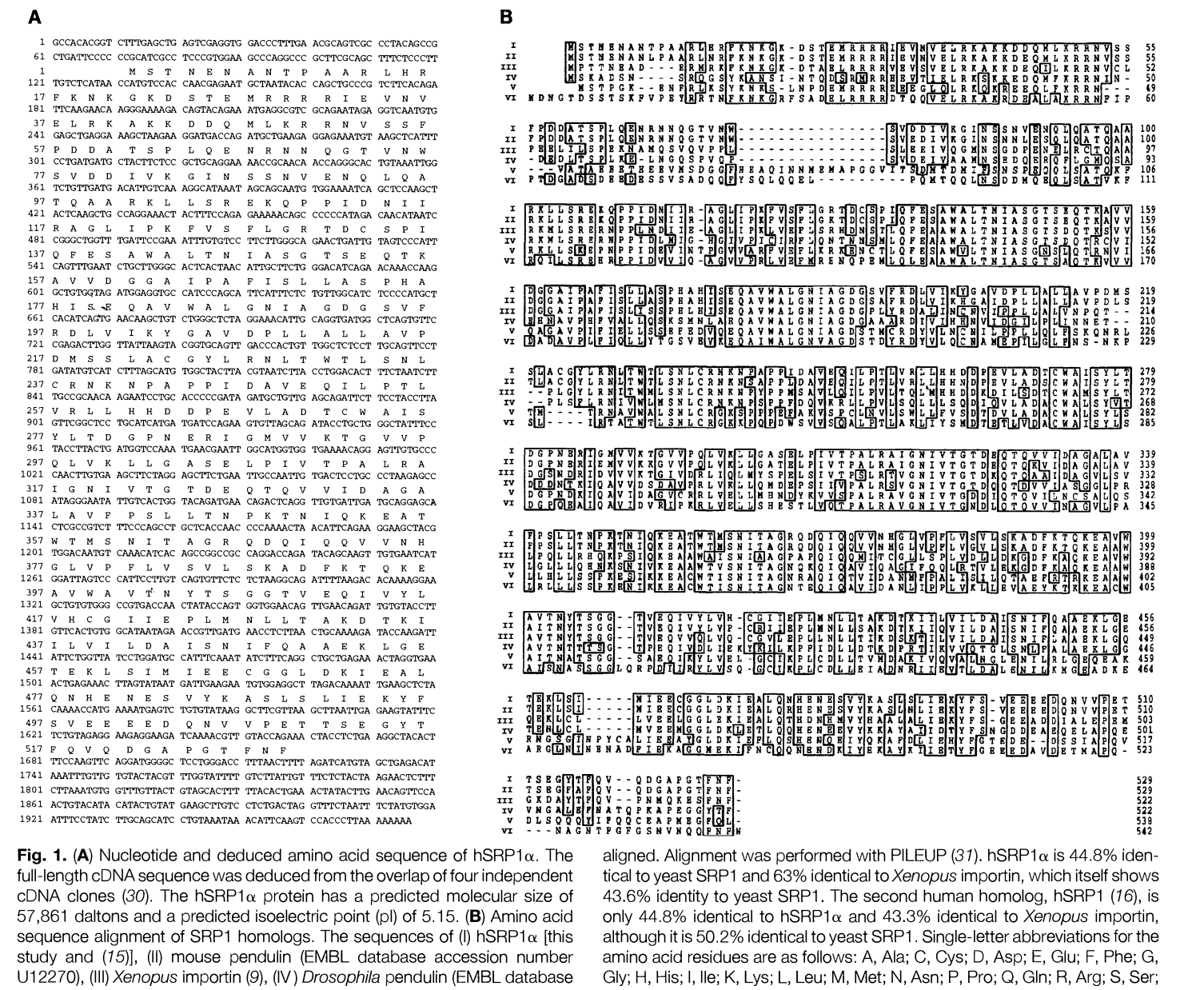

Fig. 1. (**A**) Nucleotide and deduced amino acid sequence of hSRP1α. The full-length cDNA sequence was deduced from the overlap of four independent cDNA clones (*30*). The hSRP1α protein has a predicted molecular size of 57,861 daltons and a predicted isoelectric point (pI) of 5.15. (**B**) Amino acid sequence alignment of SRP1 homologs. The sequences of (I) hSRP1α [this study and (*15*)], (II) mouse pendulin (EMBL database accession number U12270), (III) *Xenopus* importin (*9*), (IV) *Drosophila* pendulin (EMBL database accession number U12269), (V) hSRP1 (*16*), and (VI) yeast SRP1 (*10*) were aligned. Alignment was performed with PILEUP (*31*). hSRP1α is 44.8% identical to yeast SRP1 and 63% identical to *Xenopus* importin, which itself shows 43.6% identity to yeast SRP1. The second human homolog, hSRP1 (*16*), is only 44.8% identical to hSRP1α and 43.3% identical to *Xenopus* importin, although it is 50.2% identical to yeast SRP1. Single-letter abbreviations for the amino acid residues are as follows: A, Ala; C, Cys; D, Asp; E, Glu; F, Phe; G, Gly; H, His; I, Ile; K, Lys; L, Leu; M, Met; N, Asn; P, Pro; Q, Gln; R, Arg; S, Ser; T, Thr; V, Val; W, Trp; and Y, Tyr.

al proteins have been identified that bind to the NLS in vitro, but no cloned factor has been reported that fulfills the criteria of an NLS receptor (*3*).

We have carried out a yeast two-hybrid screen (*11*) with a HeLa complementary DNA (cDNA) library using the human nuclear protein p80 coilin (*12*) as the bait (*13*). Ninety positive clones were identified for further analysis. Seven clones encoded the same protein, which showed over 44% identity to yeast SRP1 (*10*). Full-length cDNAs were isolated that encoded a protein of 57.8 kD, hSRP1α (Fig. 1A). It contained eight repeats of the "arm motif" first identified in the *Drosophila armadillo* gene (*14*). The same human gene, and a second human SRP1 homolog, have also been identified on the basis of their interaction with recombination activating gene 1 (RAG1) in the two-hybrid system (*15*, *16*). The hSRP1α protein is also related to *Xenopus* importin, and a database search has revealed additional homologs in other organisms (Fig. 1B). Despite their obvious sequence similarity, the two human proteins are no more related to each other than they are to the yeast SRP1. Thus, SRP1-like proteins belong to a complex multigene family that may have similar or distinct functions. The SRP1 gene is essential in yeast, but its function has been unclear because of the pleiotropic nature of SRP1 mutant phenotypes (*10*, *17*, *18*). We found that hSRP1α could not complement a deletion in the yeast SRP1 gene (*19*).

Because p80 coilin and RAG1, which both interact with hSRP1α in the two-hybrid assay, are nuclear proteins, we tested whether hSRP1α might interact directly with nuclear localization sequences (*2*). Antibodies were raised against hSRP1α and the resulting antisera reacted with a single band of ~60 kD in a HeLa cytoplasmic extract (Fig. 2A). Immunoprecipitation with antiserum to hSRP1α (anti-hSRP1α) resulted in efficient coprecipitation of at least one other protein of ~90 kD as well as weaker recovery of several additional proteins (Fig. 2A). A number of proteins of ~30 kD were recovered with variable efficiency in different experiments. Only the 60-kD protein reacted with anti-hSRP1α in protein immunoblots (*19*). Chromatography on a MonoQ Sepharose column confirmed the association of the 60-kD (hSRP1α) and 90-kD proteins (Fig. 2A). The immunopurified complex was incubated in vitro with digoxigenin-labeled protein conjugates consisting of bovine serum albu-

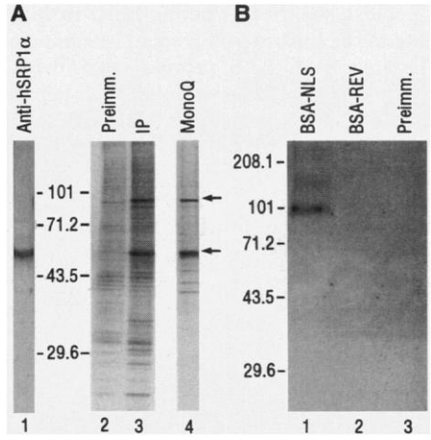

Fig. 2. (**A**) Detection and purification of native hSRP1α with specific antisera. Rabbit polyclonal antisera were raised against both recombinant hSRP1α and against a peptide corresponding to the COOH-terminal 18 amino acids of hSRP1α (*32*). The antipeptide antibody specifically reacted with a single band of ~60 kD in a HeLa cytoplasmic extract (lane 1). This antiserum was coupled to protein A–Sepharose beads and used to immunopurify native hSRP1α (*33*). As revealed by silver staining of a 10% SDS-PAGE gel, two major bands of 60 and 90 kD were immunopurified (lane 3). Neither of these proteins was recovered from Sepharose beads coupled to the preimmune serum (lane 2). Protein immunoblotting of the immunoprecipitate with anti-hSRP1α detected only the 60-kD protein (*19*). Both the 60- and 90-kD proteins copurified upon subsequent chromatography of the immunopurified complex on a MonoQ Sepharose column (*34*), as revealed by silver staining (lane 4). (**B**) Coprecipitation of digoxigenin-labeled BSA-NLS conjugate with native hSRP1α by anti-hSRP1α. Five hundred nanograms of either digoxigenin-labeled BSA-NLS or BSA-REV were incubated for 2 hours with ~100 ng of immunopurified native hSRP1α and then immunoprecipitated with anti-hSRP1α (*29*). The resulting immunoprecipitates were separated by 10% SDS-PAGE, blotted onto nitrocellulose, and probed with anti-digoxigenin coupled to alkaline phosphatase (lanes 1 to 3). The BSA-NLS conjugate is coprecipitated (lane 1) but the BSA-REV conjugate is not (lane 2). BSA-NLS is not coprecipitated by preimmune serum (lane 3) or by anti-hSRP1α in the absence of hSRP1α (*19*). Molecular sizes are indicated in kilodaltons.

min (BSA) coupled either to the functional SV40 NLS peptide (BSA-NLS) or to the reverse peptide (BSA-REV), which does not promote nuclear import (*20*), and immunoprecipitated with anti-hSRP1α (Fig. 2B). Efficient immunoprecipitation of BSA-NLS, but not BSA-REV, was observed (Fig. 2B). No BSA-NLS was recovered with either preimmune serum or in the absence of the hSRP1α fraction (Fig. 2B) (*19*). Thus, the hSRP1α–90-kD complex could bind specifically to the simple form of NLS motif.

We tested whether hSRP1α alone could bind directly to NLS motifs. Recombinant hSRP1α was expressed in *Escherichia coli* and purified to near homogeneity (Fig. 3A). It coimmunoprecipitated with BSA-NLS, but not with BSA-REV (Fig. 3B). No BSA-NLS was recovered without hSRP1α or when preimmune serum was used instead of anti-hSRP1α (Fig. 3B). The specificity of the interaction was further demonstrated by competition experiments with free SV40 NLS or REV peptides. A 50-fold molar excess of SV40 NLS peptide prevented coprecipitation of BSA-NLS by recombinant hSRP1α, whereas an equivalent molar excess of free REV peptide did not (Fig. 3C).

We then asked whether hSRP1α could also bind specifically to bipartite NLS (Fig. 3D). The human Cap-binding protein CBP80 (*21*) contains a bipartite NLS (*22*). When CBP80 was incubated with recombinant hSRP1α and immunoprecipitated with anti-hSRP1α, coprecipitation was observed (Fig. 3D). However, a transport-defective CBP80 mutant, which has a two–amino acid alteration within the bipartite NLS (*22*), was not coprecipitated (Fig. 3D). No precipitation of wild-type CBP80 was observed with preimmune serum or in the absence of recombinant hSRP1α (Fig. 3D). Using a similar assay, we observed a specific interaction between hSRP1α and recombinant nucleoplasmin (*23*), which also contains a bipartite NLS (*19*).

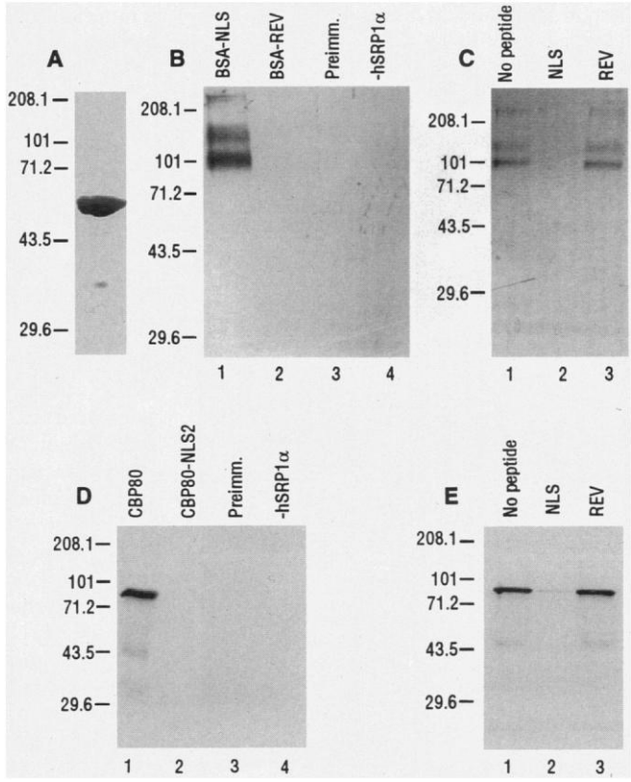

Fig. 3. (**A**) Expression and purification of recombinant hSRP1α. Histidine-tagged hSRP1α was expressed in *E. coli*, purified over Ni-NTA agarose (*35*), and its purity checked by Coomassie staining after separation on 10% SDS-PAGE. (**B**) Coprecipitation of digoxigenin-labeled BSA-NLS conjugate with recombinant hSRP1α by anti-hSRP1α. Five hundred nanograms of either digoxigenin-labeled BSA-NLS or BSA-REV were incubated with ~2 μg of recombinant hSRP1α and then immunoprecipitated with anti-hSRP1α (*34*). The resulting immunoprecipitates were separated by 10% SDS-PAGE, blotted onto nitrocellulose, and probed with anti-digoxigenin coupled to alkaline phosphatase (lanes 1 to 3). The BSA-NLS conjugate was coprecipitated (lane 1) but the BSA-REV conjugate was not (lane 2). BSA-NLS was not coprecipitated by preimmune serum (lane 3) or by anti-hSRP1α in the absence of recombinant hSRP1α (lane 4). (**C**) Coprecipitation of digoxigenin-labeled BSA-NLS conjugate competed with peptides. Digoxigenin-labeled BSA-NLS (500 ng) was incubated for 2 hours with ~2 μg of recombinant hSRP1α either in the absence of peptides (lane 1) or in the presence of a 50-fold molar excess of a peptide corresponding to the SV40 T antigen NLS (lane 2) or a 50-fold molar excess of the REV peptide (lane 3). All samples were immunoprecipitated with anti-hSRP1α and analyzed as in (B). (**D**) Coprecipitation of in vitro translated ^{35}S-labeled CBP80 with recombinant hSRP1α by anti-hSRP1α. The same amount of either wild-type (lane 1) or a transport-defective mutant of CBP80 (lane 2) was incubated for 2 hours with ~2 μg of recombinant hSRP1α and then immunoprecipitated with anti-hSRP1α (*36*). Control reactions were performed by incubation of wild-type CBP80 and hSRP1α with preimmune serum (lane 3) and incubation of wild-type type CBP80 without hSRP1α followed by immunoprecipitation with anti-hSRP1α (lane 4). The resulting immunoprecipitates were separated by 10% SDS-PAGE and analyzed with a Phosphorimager (Molecular Dynamics). (**E**) Coprecipitation of in vitro translated ^{35}S-labeled CBP80 and recombinant hSRP1α competed with peptides. Wild-type CBP80 was incubated for 2 hours with ~2 μg of recombinant hSRP1α either in the absence of peptides (lane 1) or in the presence of a 50-fold molar excess of a peptide corresponding to the SV40 T NLS (lane 2) or a 50-fold molar excess of the REV peptide (lane 3). All samples were immunoprecipitated with anti-hSRP1α and analyzed as in (D). Quantitation by the Phosphorimager indicated that the SV40 NLS peptide reduced coprecipitation by over 95% whereas the REV peptide had no inhibitory effect. Molecular sizes are indicated in kilodaltons.

Next, we tested whether hSRP1α binding to the bipartite NLS could be competed by free SV40-NLS peptide (Fig. 3E). A 50-fold molar excess of SV40 NLS peptide inhibited coprecipitation of CBP80 with hSRP1α by more than 95%, whereas an equivalent amount of the REV peptide had no effect (Fig. 3E). Thus, either the same binding site on hSRP1α interacted with both classes of NLS or two separate binding sites exist, both of which could not be occupied at the same time. Previous studies suggest that the nuclear import of proteins with both classes of NLS involve common pathways (*24, 25*). Our data suggest that recognition of NLS motifs by hSRP1α is likely to be a common step.

Xenopus importin is an essential nuclear import factor and, as discussed above, is 64% identical to hSRP1α (Fig. 1B) (9). Because the SRP1-like proteins belong to a complex multigene family, it was essential to assay whether hSRP1α, like importin, promoted the first step in nuclear protein import (that is, docking of substrate to the nuclear envelope) (Fig. 4). *Xenopus* egg extract promoted full import of a BSA-NLS conjugate in the presence of adenosine triphosphate (ATP) and an energy regeneration system (Fig. 4A) (*4, 5*). In the absence of ATP only the docking of BSA-NLS to the nuclear envelope was observed (Fig. 4B). No docking or import was observed in the absence of extract or in the presence of recombinant Ran alone (Fig. 4, C and E). Addition of recombinant hSRP1α instead of *Xenopus* extract promoted docking, but not import, of BSA-NLS (Fig. 4D). The hSRP1α-mediated docking depended on the presence of a functional NLS in the import substrate, but was independent of ATP and an energy regeneration system (*19*). Addition of both recombinant hSRP1α and recombinant Ran mediated complete import of BSA-NLS into the nucleus (Fig. 4F). Thus, two recombinant human proteins are sufficient to reconstitute nuclear protein import in this in vitro assay system. Because the efficiency of import was lower with the two purified components than with the total extract, other factors or protein modifications, or both, might also be involved in protein import. Candidate factors would include the 90-kD protein associated with endogenous hSRP1α, and pp15, which together with Ran constitutes import fraction B (*8*).

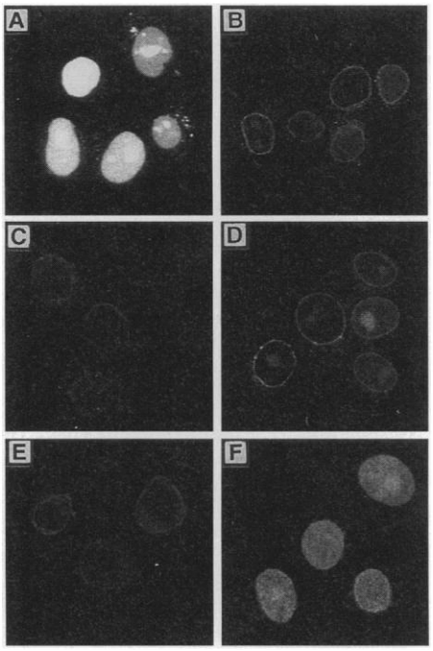

Fig. 4. In vitro nuclear protein import assays. Import of fluorescein-coupled BSA-NLS conjugate into nuclei of digitonin-permeabilized HeLa cells (*37*) was assayed in the presence of either *Xenopus* egg extract (10 mg/ml final concentration) (**A** and **B**), no extract (**C**), recombinant hSRP1α alone (200 μg/ml final concentration) (**D**), recombinant human Ran alone (200 μg/ml final concentration) (**E**), and both recombinant hSRP1α and Ran together (**F**). Pictures were recorded with a confocal fluorescence microscope. ATP, GTP, creatine phosphate, and creatine kinase were included in the assays shown in (A) and (C) and in (D) through (F). Similar results to those shown in (D) were obtained also in the absence of the NTPs and creatine phosphate and kinase (*19*). As previously observed, nucleolar staining was frequently present in the import assays (*5, 9*). In the assay shown in (B), no NTPs or creatine phosphate or creatine kinase were added and hexokinase was included to deplete endogenous NTPs.

It is likely that hSRP1α is part of a larger complex in vivo because it is associated with at least one other protein of 90 kD. Although its function is unknown, the 90-kD protein might modulate the binding of hSRP1α to NLS motifs, mediate interactions with other components of the transport machinery, or both. Two bovine factors, corresponding to previously identified NLS-binding components of 54 and 56 kD (*26*), and a factor of ~97 kD combine to promote the first step in nuclear import in vitro (*27*). Similarly, a second labile subunit of *Xenopus* importin can be detected, consistent with its activity as part of a larger complex in vivo (*9*).

A putative function for the yeast SRP1 protein in the nuclear import of proteins could account for the complexity of its mutant phenotypes (*10, 17*). Both genetic and immunofluorescence data in yeast indicate that SRP1 interacts with nuclear pore components (*10, 18*). At least one other class of NLS receptor is believed to mediate import of small nuclear ribonucleoprotein particles (snRNPs) (*24, 28*). Perhaps other members of the SRP1 gene family might bind this class of nuclear import substrate or bind to proteins with different forms of the NLS motif.

REFERENCES AND NOTES

1. W. D. Richardson, A. D. Mills, S. M. Dilworth, R. A. Laskey, C. Dingwall, *Cell* **52**, 655 (1988); D. D. Newmeyer and D. J. Forbes, *ibid.*, p. 641; P. A. Silver, *ibid.* **64**, 489 (1991); L. Gerace, *Curr. Opin. Cell Biol.* **4**, 637 (1992).
2. C. Dingwall and R. A. Laskey, *Trends Biochem. Sci.* **16**, 478 (1991).
3. L. Yamasaki and R. E. Lanford, *Trends Cell Biol.* **2**, 123 (1992).
4. S. A. Adam, R. S. Marr, L. Gerace, *J. Cell Biol.* **111**, 807 (1990).
5. M. S. Moore and G. Blobel, *Cell* **69**, 939 (1992).
6. ———, *Nature* **365**, 661 (1993).
7. F. Melchior *et al.*, *J. Cell Biol.* **123**, 1649 (1993).
8. M. S. Moore and G. Blobel, *Proc. Natl. Acad. Sci. U.S.A.* **91**, 10212 (1994).
9. D. Görlich, S. Prehn, R. A. Laskey, E. Hartmann, *Cell* **79**, 767 (1994).
10. R. Yano, M. Oakes, M. Yamaghishi, J. A. Dodd, M. Nomura, *Mol. Cell. Biol.* **12**, 5640 (1992).
11. S. Fields and O. Song, *Nature* **340**, 245 (1989).
12. L. E. Andrade *et al.*, *J. Exp. Med.* **173**, 1407 (1991).
13. The yeast two-hybrid screen was performed as described [A. S. Zervos, J. Gyuris, R. Brent, *Cell* **72**, 223 (1993)] with a HeLa cDNA library. Ninety positive clones were identified of which seven corresponded to hSRP1α and are analyzed here. A detailed analysis of the other positive clones will be presented elsewhere.
14. B. Riggleman, E. Wieschaus, P. Schedl, *Genes Dev.* **3**, 96 (1989); M. Pfeifer, S. Berg, A. B. Reynolds, *Cell* **76**, 789 (1994).
15. C. A. Cuomo, S. A. Kirch, J. Gyuris, R. Brent, M. A. Oettinger, *Proc. Natl. Acad. Sci. U.S.A.* **91**, 6156 (1994).
16. P. Cortes, Z. S. Ye, D. Baltimore, *ibid.*, p. 7633.
17. R. Yano, M. L. Oakes, M. M. Tabb, M. Nomura, *ibid.*, p. 6880.
18. K. D. Belanger, M. A. Kenna, S. Wei, L. I. Davis, *J. Cell Biol.* **126**, 619 (1994).
19. K. Weis, I. W. Mattaj, A. I. Lamond, unpublished observations.
20. S. A. Adam, T. J. Lobl, M. A. Mitchell, L. Gerace, *Nature* **337**, 276 (1989).
21. E. Izaurralde, J. Stepinski, E. Darzynkiewicz, I. W. Mattaj, *J. Cell Biol.* **118**, 1287 (1992); E. Izaurralde *et al.*, *Cell* **78**, 657 (1994); N. Kataoka, M. Ohno, K. Kangawa, Y. Tokoro, Y. Shimura, *Nucleic Acids. Res.* **22**, 3861 (1994).
22. CBP80 contains a bipartite NLS with the sequence RRRHSDENDGGQPHKRRK. A two–amino acid change in this NLS (RRRHSDENDGGQPHAARK) was shown to prevent nuclear import of the CBP80 protein (E. Izaurralde, C. McGuigan, I. W. Mattaj, unpublished data).
23. C. Dingwall *et al.*, *EMBO J.* **6**, 69 (1987).
24. N. Michaud and D. S. Goldfarb, *J. Cell Biol.* **112**, 215 (1991).
25. ———, *Exp. Cell Res.* **208**, 128 (1993).
26. S. A. Adam and L. Gerace, *Cell* **66**, 837 (1991).
27. E. J. Adam and S. A. Adam, *J. Cell Biol.* **125**, 547 (1994).
28. U. Fischer *et al.*, *EMBO J.* **10**, 705 (1991).
29. We performed coprecipitation assays by mixing either the hSRP1α complex or the recombinant protein with digoxigenin-labeled BSA conjugated to either the SV40 NLS or REV peptides and incubating the mixture in 100 μl of IPP buffer [150 mM NaCl, 20 mM tris-HCl (pH 7.6), 0.1% Triton X-100] for 2 hours at 4°C. Five microliters of either rabbit preimmune or immune serum were added and incubated for 1 hour at 4°C followed by addition of a 20-μl packed volume of protein A beads and incubated for a further hour at 4°C. Beads were washed three times with 1 ml of IPP buffer and proteins were recovered by boiling in sample buffer and then analyzed by 10% SDS–polyacrylamide gel electrophoresis (PAGE).
30. Additional hSRP1α cDNA clones were obtained by hybridization screening of a second HeLa cDNA library and used to assemble the full-length cDNA sequence shown in Fig. 1A.
31. J. Devereux, P. Haeberli, O. Smithies, *Nucleic Acids. Res.* **12**, 387 (1984).
32. Rabbit antibodies were raised against the hSRP1α

peptide SEGYTFQVQDGAPGTFNF coupled to keyhole limpet hemocyanin and against full-length recombinant hSRP1α expressed in *E. coli* (Fig. 3A). Standard immunization procedures were used.
33. Immunopurification was performed by recycling 10 ml of HeLa S100 extract (~10 mg/ml), prepared according to the method described by Dignam *et al.* [J. D. Dignam, R. M. Lebovitz, R. G. Roeder, *Nucleic Acids. Res.* **11**, 1475 (1983)], over a 1-ml column of protein A–Sepharose 4B beads (Pharmacia) coupled to either preimmune or antipeptide antiserum, for 2 hours at 4°C. The beads were washed with 50 ml of IPP buffer and then eluted by incubation of the beads for 2 hours at room temperature in 1 ml of IPP buffer containing free hSRP1α peptide (1 mg/ml).
34. For MonoQ chromatography, eluates of the affinity column were dialyzed for 2 hours at 4°C against 500 ml of IPP buffer without Triton X-100 and peptide. The dialyzate was loaded directly onto a MonoQ PC1.6/5 column through use of the SMART system (Pharmacia) and eluted with a gradient from 150 to 600 mM NaCl in 20 column volumes. The hSRP1α complex eluted in a sharp peak at ~300 mM NaCl.
35. The hSRP1α expression vector was constructed by subcloning of a Bam HI–Xho I fragment of a Bluescript plasmid vector containing the full-length hSRP1α cDNA (pBShSRP1α) inserted between the Bam HI and Xho I sites of the His vector pRSET (Invitrogen). The resulting plasmid, pHish-SRP1α, was grown in *E. coli* strain BL21LysS to an absorbance at 600 nm (A_{600}) of 0.4 and induced with isopropyl-β-D-thiogalactopyranoside for 3 hours at 30°C. Cells from a 3-liter culture were lyzed with a French Press and recombinant hSRP1α purified twice over Ni–nitrilotriacetic acid agarose (Qiagen) under native conditions.
36. Immunoprecipitations were done as described (*29*). ^{35}S-labeled CBP80 and CBP80-NLS2 were prepared by in vitro translation with rabbit reticulocyte lysate (Promega).
37. Import assays were done essentially as described by Adam *et al.* (*4*) except that HeLa cells were permeabilized in suspension with digitonin. All samples were incubated at 23°C for 60 min in a total volume of 10 μl in a buffer containing 20 mM Hepes-KOH (pH 7.3), 110 mM potassium acetate, 5 mM sodium acetate, 2 mM magnesium acetate, 1 mM EGTA, 2 mM dithiothreitol, 1 mM phenylmethylsulfonyl fluoride (all final concentrations) with ~10^4 cells per assay. The samples indicated contained ATP and GTP (guanosine triphosphate) (each at 2 mM), creatine phosphate (10 mM), and creatine kinase (1 μg/ml) (all final concentrations). Hexokinase was used at 20 U/ml final concentration. *Xenopus* egg extracts were prepared essentially as described [M. J. Lohka and Y. Masui, *Science* **220**, 719 (1984)].
38. We are grateful to C. Dingwall, E. Izaurralde, I. Palacios, and C. McGuigan for discussions and help with the in vitro transport assays and for sharing reagents. We are also grateful to R. Brent and T. Kreis for providing HeLa cDNA libraries, to J. Lewis for help with fractionation procedures, and to M. Nomura for providing yeast strains. We thank C. Calvio, S. Kandels-Lewis, G. Lamm, N. Santama, B. Seraphin, and our other colleagues for helpful discussions and for critical comments on the manuscript. K.W. was supported by a predoctoral stipend from Boehringer Ingelheim Fonds.

26 January 1995; accepted 6 March 1995

Photovoltage of Rods and Cones in the Macaque Retina

David M. Schneeweis and Julie L. Schnapf*

The kinetics, gain, and reliability of light responses of rod and cone photoreceptors are important determinants of overall visual sensitivity. In voltage recordings from photoreceptors in an intact primate retina, rods were found to be functionally isolated from each other, unlike the tightly coupled rods of cold-blooded vertebrates. Cones were observed to receive excitatory input from rods, which indicates that the cone pathway also processes rod signals. This input might be expected to degrade the spatial resolution of mesopic vision.

The photocurrent signals of photoreceptor cells primarily reflect light-activated biochemical processes that occur in the outer segment. The membrane potential, however, also can be shaped by voltage-dependent conductances and synaptic interactions (*1*). This study demonstrates a role for these latter processes in primate photoreceptors. These processes are of particular importance because the photovoltage, not the photocurrent, modulates synaptic transmission.

Photovoltage responses of 16 rods and 23 cones (14 green and 9 red) from 13 monkeys were measured with the perforated-patch technique (*2*). Dark-adapted retinas, obtained primarily from the monkey *Macaca fascicularis*, were placed in a recording chamber and superfused with physiological saline (*3*). A 180- or 400-μm-diameter spot of plane-polarized light, incident on the ganglion cell side of the retina, was focused onto the photoreceptors. The rate of photoisomerization was estimated from the product of the light intensity and the collecting area, A_c, of the photoreceptor (*4*).

The dark resting potential of rods was, on average, −37 mV, and light evoked hyperpolarizing responses that increased with flash strength (Fig. 1, A and B). The relation between peak hyperpolarization and photon density was fitted by a Michaelis function (Fig. 1C). This function is less steep than the exponential saturation function that describes the intensity dependence of the photocurrent in macaque and human rods (*5*, *6*). The photon density that elicited a response of half-maximal amplitude was 75 ± 40 photons μm^{-2} (mean ± SD, n = 10), or about 75 photoisomerizations. Input resistance was 1.2 ± 0.5 gigohms (mean ± SD, n = 6) (*7*).

The time to the peak of the response to the flash decreased with increasing flash strength from 200 ms to less than 35 ms (Fig. 1, A and B). In response to bright flashes, the photovoltage displayed an initial transient that decayed to a plateau of intermediate value. These kinetic features are not present in the photocurrent (*5*); differences of this kind between photocurrent and voltage have been observed previ-

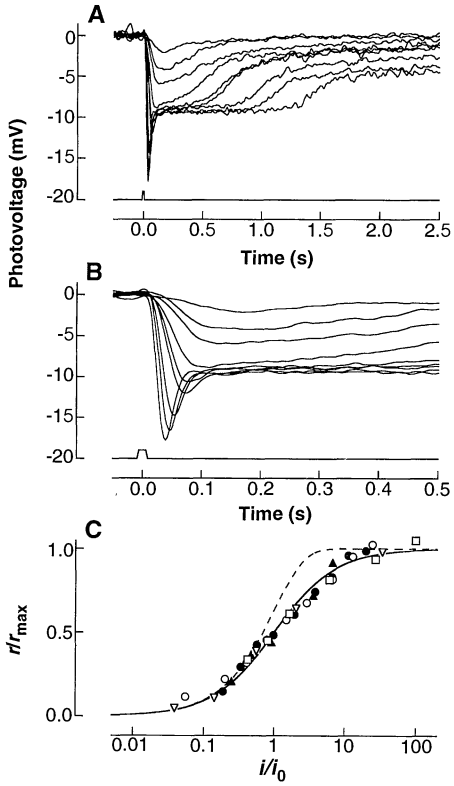

Fig. 1. Dependence of photovoltage on flash strength in macaque rods. Change in membrane potential in one rod is plotted in (**A**) and (**B**), on two time scales, as a function of time after the middle of a 10-ms flash. Traces are average responses to 1 to 18 flashes. Dark resting membrane potential is −43 mV. Response bandwidth, DC to 30 Hz. Flash monitor is below voltage traces. Flash photon densities ranged from 5 photons μm^{-2} to 2300 photons μm^{-2}, at 500 nm. (**C**) Peak hyperpolarization of five rods is plotted as a function of flash strength on normalized axes. Each symbol represents a different cell; r, peak hyperpolarization; r_{max}, maximal hyperpolarization to a saturating light; i, flash photon density; i_0, the photon density that elicited a peak response of ½r_{max}. For the cells plotted, r_{max} varied between 13 mV and 35 mV (mean 22 mV) and i_0 ranged from 17 photons μm^{-2} to 130 photons μm^{-2}. The continuous curve is the Michaelis function, $r/r_{max} = i/(i + i_0)$; the dashed curve is an exponential saturation function, $r/r_{max} = 1 - \exp(-i/i_0)$.

Departments of Ophthalmology and Physiology, University of California, San Francisco, CA 94143–0730, USA.

*To whom correspondence should be addressed.